^{223}Ra Induces Transient Functional Bone Marrow Toxicity

Maria Parlani*[1], Francesco Boccalatte*[2], Anna Yeaton[2], Feng Wang[3], Jianhua Zhang[3], Iannis Aifantis[2], and Eleonora Dondossola[1]

[1]*Genitourinary Medical Oncology Department and David H. Koch Center for Applied Research of Genitourinary Cancers, University of Texas M.D. Anderson Cancer Center, Houston, Texas;* [2]*Department of Pathology and Laura and Isaac Perlmutter Cancer Center, New York University School of Medicine, New York, New York; and* [3]*Department of Genomic Medicine, University of Texas M.D. Anderson Cancer Center, Houston, Texas*

^{223}Ra is a bone-seeking, α-particle–emitting radionuclide approved for the treatment of patients with metastatic prostate cancer and is currently being tested in a variety of clinical trials for primary and metastatic cancers to bone. Clinical evaluation of ^{223}Ra hematologic safety showed a significantly increased rate of neutropenia and thrombocytopenia in patients, hinting at myelosuppression as a side effect. **Methods:** In this study, we investigated the consequences of ^{223}Ra treatment on bone marrow biology by combining flow cytometry, single-cell RNA sequencing, three-dimensional multiphoton microscopy and bone marrow transplantation analyses. **Results:** ^{223}Ra accumulated in bones and induced zonal radiation damage confined to the bone interface, followed by replacement of the impaired areas with adipocyte infiltration, as monitored by 3-dimensional multiphoton microscopy ex vivo. Flow cytometry and single-cell transcriptomic analyses on bone marrow hematopoietic populations revealed transient, nonspecific ^{223}Ra-mediated cytotoxicity on resident populations, including stem, progenitor, and mature leukocytes. This toxicity was paralleled by a significant decrease in white blood cells and platelets in peripheral blood—an effect that was overcome within 40 d after treatment. ^{223}Ra exposure did not impair full hematopoietic reconstitution, suggesting that bone marrow function is not permanently hampered. **Conclusion:** Our results provide a comprehensive explanation of ^{223}Ra reversible effects on bone marrow cells and exclude long-term myelotoxicity, supporting safety for patients.

Key Words: ^{223}Ra; myelotoxicity; bone marrow

J Nucl Med 2022; 63:1544–1550
DOI: 10.2967/jnumed.121.263310

The radioisotope ^{223}Ra is an α-particle emitter that accumulates in bone after in vivo administration (*1,2*). ^{223}Ra was originally tested as targeted radiotherapy for prostate cancer metastasis in bone (*1*), which represents a major site for distant colonization (*3*). The high-energy radiation of ^{223}Ra, coupled with limited penetrance in tissues (<100 μm), mediates zonal toxicity at the bone interface toward osteoblasts, osteoclasts, and tumor cells (*4–7*). ^{223}Ra prolonged the median overall survival (3.6 mo) and delayed the time to first symptomatic skeletal event (5.8 mo) in men with prostate cancer metastatic to bone (*8,9*). These results led to the approval of ^{223}Ra for the treatment of metastatic prostate cancer patients with symptomatic bone lesions and no visceral involvement (*8,9*). On the basis of this positive outcome, the use of ^{223}Ra is now being clinically investigated for other tumor types that colonize the bone, including multiple myeloma, hormone-positive breast cancer, renal cell carcinoma, non–small cell lung cancer, and differentiated thyroid cancer (*10–12*).

Follow-up studies on patients excluded long-term emergence of secondary malignancies associated with ^{223}Ra treatment (such as other primary bone cancers or acute myelogenous leukemia) for up to 3 y (*13,14*). Hematologic safety analyses instead showed an impact by ^{223}Ra on bone marrow function (*15*). Accordingly, median absolute neutrophil counts and platelet number, which remained constant for placebo-treated patients, significantly decreased in ^{223}Ra-treated men, with a rebound after the end of the treatment. Hemoglobin levels were not significantly affected over the treatment period in either the ^{223}Ra group or the placebo group. In comparison, antitumor radiation levels of β-emitting agents such as ^{89}Sr- or ^{153}Sm-ethylenediamine-tetra-methylene-phosphonic acid, which displays abundant γ-emission, are associated with more severe bone marrow toxicity, limiting their usefulness for treating patients (*1*).

Neutropenia and thrombocytopenia currently represent the most common adverse reactions and hint at significant levels of bone marrow toxicity (*15*). Therefore, understanding the biologic determinants of ^{223}Ra-mediated myelosuppression and the medium- to long-term consequences on bone marrow function is critical to support a more meaningful and rational application of this agent in current and future patients. Furthermore, ruling out major toxic effects could further prompt ^{223}Ra use in early-stage patients.

In this study, we investigated the effects of ^{223}Ra on bone marrow biology, including topology and function. We applied preclinical murine models combined with 3-dimensional multiphoton microscopy, flow cytometry analysis, bone marrow transplantation experiments, and single-cell RNA sequencing to elucidate ^{223}Ra-mediated myelotoxicity over time.

MATERIALS AND METHODS

Animal Studies

Animal studies were approved by the Institutional Animal Care and Use Committee of the University of Texas M.D. Anderson Cancer Center and were performed according to the institutional guidelines for animal care and handling. More details on the in vivo studies are provided in the supplemental materials (available at http://jnm.snmjournals.org).

Statistical Analysis

Statistical analysis was performed using GraphPad Prism 8 by unpaired 2-tailed Student *t* testing or 1-way ANOVA followed by

Received Oct. 13, 2021; revision accepted Feb. 10, 2022.
For correspondence or reprints, contact Eleonora Dondossola (edondossola@mdanderson.org) or Francesco Boccalatte (francesco.boccalatte@nyulangone.org).
*Contributed equally to this work.
Published online Feb. 17, 2022.

Tukey post hoc testing. Data are mean ± SD. For single-cell RNA sequencing, differential expression analysis was determined using the Wilcoxon rank sum test.

Further experimental methods are detailed in the supplemental materials.

RESULTS

^{223}Ra Accumulates in Bones and Affects the Bone Marrow Compartment

To study the effects of ^{223}Ra on bone marrow biology, C57BL/6 mice were administered a single dose of 7.5 kBq, according to the therapeutic dose used in other preclinical analyses on mice (*2,4,6*). Radiation emission was monitored for up to 40 d in femur, tibia, humerus, skull, and spine. ^{223}Ra accumulated in different bones and significantly decayed over time to a similar extent, with limited radiation emission (≤15% of the initial amount) detectable by day 40 after injection, in line with its half-life of 11.4 d (Fig. 1A) (*1*). Bone matrix showed localized radioactivity, whereas no signal was detected within bone marrow cells (Fig. 1A). These results confirm that ^{223}Ra accumulates in calcified bone tissues but not in the bone marrow cavity, as previously reported (*2*). Interestingly, ^{223}Ra induced a significant decrease in white blood cells in bone, whereas levels of red blood cells and platelets did not significantly change (Fig. 1B). These results suggest that ^{223}Ra incorporates in the calcified component of bone and induces cellular changes in bone marrow cells.

^{223}Ra Induces Topologic Changes Within the Bone Marrow Cavity

Next, we investigated the topologic effects that ^{223}Ra exerts over time on bone marrow cells by applying infrared-excited nonlinear microscopy. We focused on tibia, which recapitulates the complexity of bone architecture, including areas of cancellous bone at the distal epiphysis/metaphysis (where ^{223}Ra effects should be maximized (*2*)), and a trabecula-free cavity at the diaphysis (where the impact of ^{223}Ra should be minimal (*2*)). Tibiae were processed, cut at the vibratome to generate 3-dimensional slices, stained, and analyzed by multiphoton microscopy. We acquired 3-dimensional stacks (up to 4.5 mm × 1.2 mm × 200 mm) at different time points and monitored bone marrow cells (CD45, a marker expressed by all nucleated hematopoietic cells (*16*), and 4′,6-diamidino-2-phenylindole), together with second- and third-harmonic generation label-free nonlinear imaging techniques. Second-harmonic generation is elicited by noncentrosymmetric structures, such as collagen deposited in the bone matrix (*4*), whereas third-harmonic generation is engendered at different interfaces, such the water-lipid interface in adipocytes (*17*). Bone marrow at the baseline showed a homogeneous distribution of CD45$^+$ cells, intercalated within bone trabeculae at the epiphysis and metaphysis, with no evidence of adipocytes, as expected for healthy adult mice younger than 2 y (Fig. 2A; Supplemental Fig. 1A) (*20*). By day 4 after ^{223}Ra injection, bone marrow at the epiphysis and metaphysis showed major damage, with CD45-positive cells alternated to strongly fluorescent circular structures, negative for third-harmonic generation (Fig. 2A; Supplemental Fig. 1B). These events preferentially localized at 36.6 ± 36 μm from bone, either trabecular or cortical, and were distributed mostly at the epiphysis or metaphysis, within 1.39 mm (Fig. 2B) from the growth plate. By day 11, active damage persisted near cancellous and cortical bone, with preferential distribution 2,247 ± 700 μm from the growth plate, paralleled by the emergence

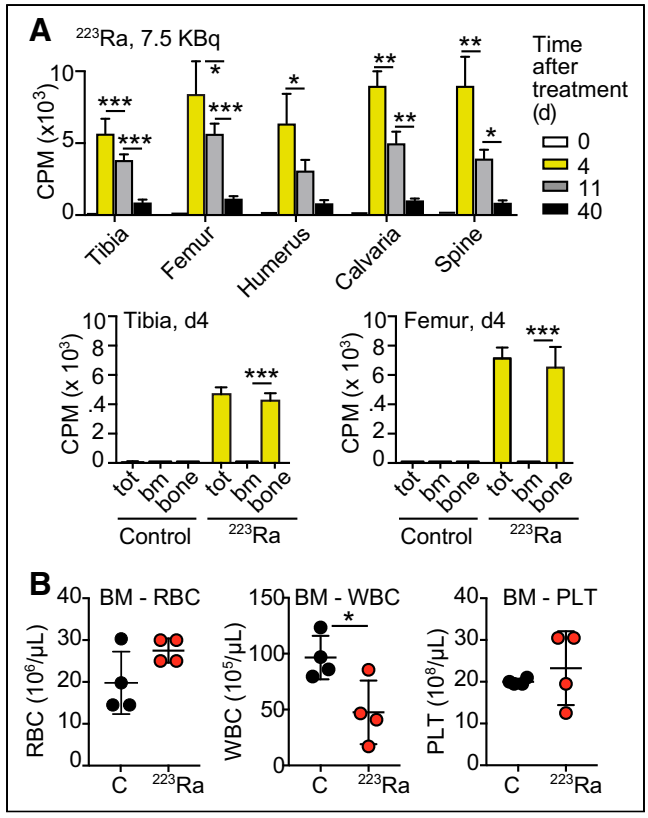

FIGURE 1. ^{23}Ra accumulates in bones and affects bone marrow compartment. (A, top) Measurement of radiation emission by ^{223}Ra-treated bones over time. Tibia, femur, humerus, calvaria, and spine were removed at 0, 4, 11, or 40 d after ^{223}Ra treatment, and counts per minute were measured. Mean ± SD is shown (3–6 bones per group). *$P < 0.05$. **$P < 0.01$. ***$P < 0.001$. Significance was tested on 1-way ANOVA followed by Tukey honestly-significant-difference post hoc test. (A, bottom) Tibia and femur from control mice or 4 d after ^{223}Ra treatment were removed, and counts per minute were measured for total bone or mineralized bone and bone marrow separately, after bone marrow flushing. Mean ± SD is shown (4 bones per group). ***$P < 0.001$ by unpaired 2-tailed Student *t* test. (B) Bone marrow hematologic analysis of control and ^{223}Ra (day 4)-treated mice by ABX Micros 60 hematology analyzer. Mean ± SD is shown (4 mice per group). *$P < 0.05$ by unpaired 2-tailed Student *t* test. bm and BM = bone marrow; bone = mineralized bone; CPM = counts per minute; PLT = platelets; RBC = red blood cells; tot = total bone; WBC = white blood cells.

of third-harmonic generation-positive adipocytes at the epiphysis and metaphysis (Fig. 2; Supplemental Fig. 1C). This trend increased until up to day 40 (Fig. 2A; Supplemental Fig. 1D), with a significantly higher number of third-harmonic generation–positive adipocytes at the epiphysis and metaphysis and some damage still persisting at the metaphysis (Fig. 2B). By day 60, fewer than 5 areas of damage per slice were still visible, with a significant infiltration of adipocytes at the epiphysis and metaphysis (Fig. 2B; Supplemental Fig. 1E). The bone marrow at the diaphysis instead did not show any sign of perturbation, even on day 4 after treatment, when the damage was more evident in other areas (Fig. 2; Supplemental Figs. 1A–1E). The progressive adipocyte increase at the epiphysis and metaphysis, with no involvement of the diaphysis, was further confirmed by histology (Supplemental Fig. 2).

These results suggest that ^{223}Ra induces extensive bone marrow remodeling at the epiphysis and metaphysis, which are more

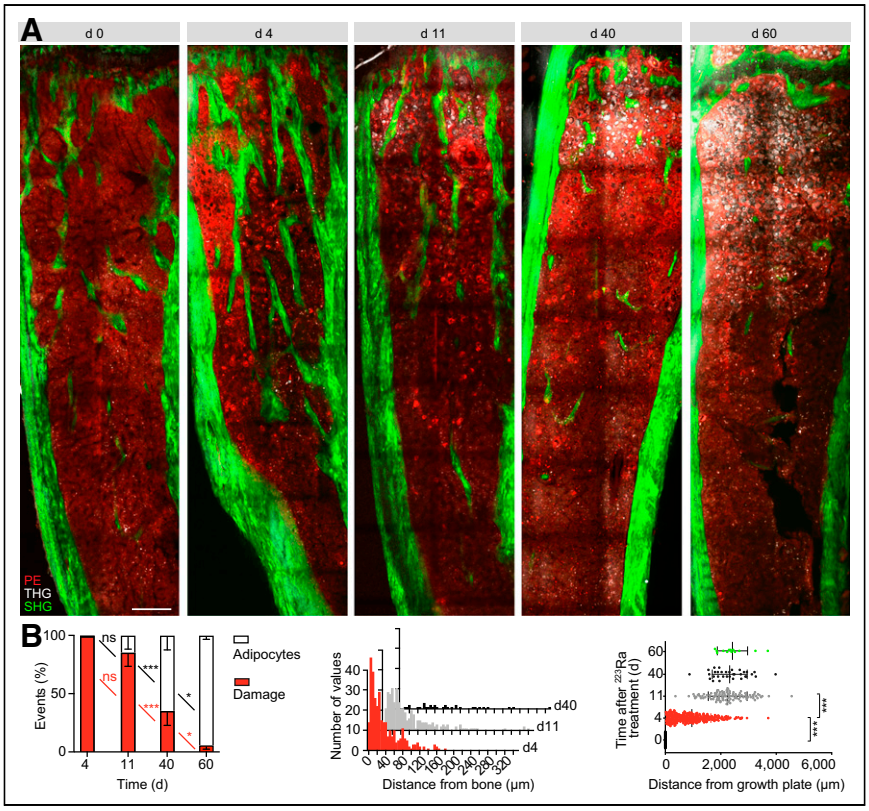

FIGURE 2. ^{223}Ra induces topologic changes within bone marrow cavity. (A) Immunofluorescence analysis of 4.5 mm × 1.2 mm × 200 μm tibia slices retrieved from mice before and 4, 11, 40, and 60 d after ^{223}Ra treatment. Red indicates CD45-positive cells, PE; gray indicates adipocytes, third-harmonic generation; green indicates bone, second-harmonic generation. Scale bar is 300 μm. (B, left) Percentage of radiation damage events and adipocytes in tibia slices on days 0–60 after ^{223}Ra treatment. Mean ± SD is shown, with total number of events reported for 1 slice per tibia, 1 tibia per mouse, and 3 mice per group. (B, middle) Frequency distribution of radiation-damage-event distance from bone on days 4, 11, and 40 for 1 slice per tibia, 1 tibia per mouse, and 3 mice per group. (B, right) Distance of radiation damage events from growth plate on days 0–60 after ^{223}Ra treatment. Mean ± SD is shown, with total number of events reported for 1 slice per tibia, 1 tibia per mouse, and 3 mice per group. *$P < 0.05$. ***$P < 0.001$. Significance was tested on 1-way ANOVA followed by Tukey honestly-significant-difference post hoc test. ns = not statistically significant; PE = R-phycoerythrin; SHG = second-harmonic generation; THG = third-harmonic generation.

exposed to its radiation, possibly because of the presence of cancellous bone, but leaves the diaphysis morphologically unperturbed.

^{223}Ra Induces Transient, Nonspecific Myelotoxicity in Bone Marrow-Derived Cells

To evaluate the effects of ^{223}Ra on specific bone marrow populations, mice were treated with ^{223}Ra and their bone marrow collected either before (day 0) or at 4, 11, and 40 d after treatment. Then, the impact of ^{223}Ra on stem, progenitor, mature leukocyte, and erythroid cells was evaluated by flow cytometry (Supplemental Fig. 3; Supplemental Table 1). To further evaluate the long-term toxicity, we monitored hematopoietic stem and progenitor cells at various stages of differentiation. ^{223}Ra treatment significantly depleted total CD45-positive bone marrow leukocytes at 4 and 11 d after treatment, whereas their number returned to baseline after 40 d, indicating a transient effect (Fig. 3A; Supplemental Fig. 4A). When we monitored hematopoietic stem and progenitor cells at various stages of differentiation, we found that the early myeloid and lymphoid lineages were affected to a similar extent (Fig. 3A; Supplemental Figs. 4B and 4C). Notably, the long-term hematopoietic stem cell (HSC) population (Lin-negative Kit-positive Sca-positive CD135-negative CD150-positive CD40-negative) was also significantly reduced by ^{223}Ra but fully recovered by 40 d after treatment, suggesting restoration of the hematopoiesis and reversible myelotoxicity. This was further confirmed by the evaluation of mature myeloid and lymphoid cells, which reached normal levels by 40 d after treatment (Fig. 3A; Supplemental Fig. 4D). The only cell type not significantly affected by ^{223}Ra treatment was mature erythrocytes. To better understand the nature of this phenomenon, we further dissected this population according to the maturation stages and identified depletion of the more immature precursors and erythroblasts by early ^{223}Ra treatment, whereas the mature, nonnucleated erythrocytes (which are the most abundant population) were unaffected by ^{223}Ra (Fig. 3A; Supplemental Fig. 4E). The absence of splenomegaly for up to day 40 after treatment suggests that no extramedullary hematopoiesis emerged to compensate the bone marrow functional damage (Fig. 3B). Analysis of peripheral blood at different time points after ^{223}Ra treatment showed a significant decrease in white blood cells until up to day 28 after treatment, as well as a significant decrease in platelets until up to day 16 after treatment, and no significant reduction in red blood cells, hemoglobin, or hematocrit (Fig. 3C), in agreement with the outcome observed in patients (*15*).

These results indicate that in multiple bone marrow populations, treatment with ^{223}Ra has widespread toxicity that resolves over time. To evaluate the global effects of ^{223}Ra on bone marrow in early hematopoietic populations, we conducted single-cell RNA sequencing on Kit-positive hematopoietic stem and progenitor cells from the bone marrow of C57BL/6 mice over time (days 0, 4, 11, and 40 after treatment with ^{223}Ra; 3 mice per time point). We obtained high-quality transcriptomic data from a total of 10,501 single cells followed by analysis using Seurat, an R package designed for single-cell RNA sequencing data (*18*). The distribution of all the transcriptomes over time was visualized using uniform manifold approximation and projection (Fig. 4A). To define similarity clusters, we applied unsupervised clustering based on the differential expression analysis for specific genes with a resolution of 0.8 and resolved 26 separate clusters (Supplemental Figs. 5 and 6). On the basis of previous studies on single-cell gene expression (*19*), we manually curated population-specific genes in each cluster and defined 16 distinct populations, comprising all major stem, progenitor, and mature bone marrow cell types (Fig. 4A). In particular, to guide a reliable cell type assignment, we examined the expression of specific genes correlating with a more primitive (CD34, Flt3) or more lineage-primed (Dntt, Elane, Ly6g) phenotype (Fig. 4B; Supplemental Fig. 7). By comparing the bone marrow composition at baseline and after ^{223}Ra treatment over time, we observed that the most primitive cluster of hematopoietic stem

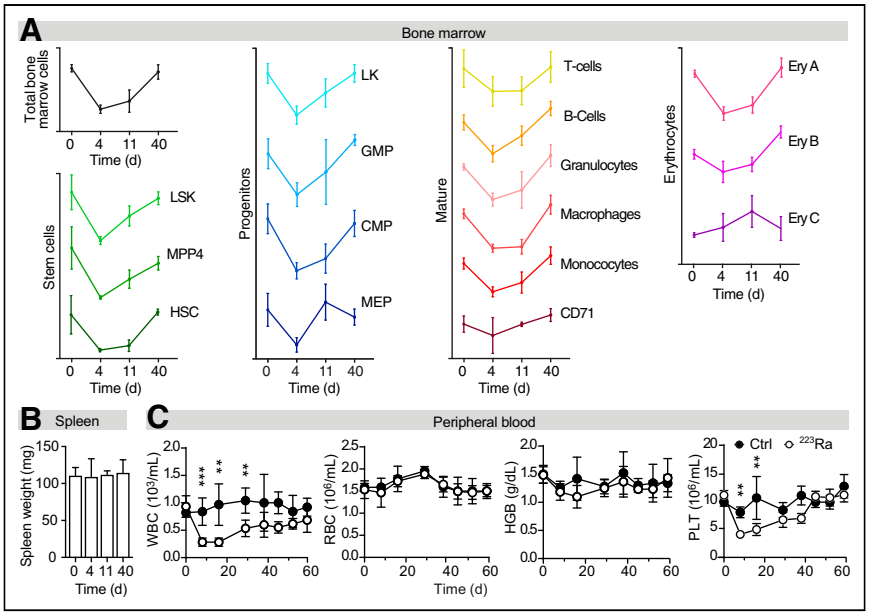

FIGURE 3. ^{223}Ra causes significant but transient myelotoxicity. (A) Effects of ^{223}Ra treatment at baseline and after 4, 11, and 40 d on total bone marrow leukocytes; hematopoietic stem and progenitor cells (based on LSK, MPP4, or HSC markers); early progenitor cells (based on LK, granulocyte-macrophage progenitor, common myeloid progenitor, and megakaryocyte-erythrocyte progenitor markers); B, T, myeloid, and erythroid markers; and erythroid cells at different stages of maturation for 3–4 mice/group. One representative experiment is shown, and experiment was repeated twice. Absolute numbers for each graph and statistical analysis are reported in Supplemental Figure 4. (B) Spleen weight (4 spleens per group). (C) Hematologic analysis of control and ^{223}Ra-treated mice on days 0–60 after treatment for 5–6 mice per group. One representative experiment is shown, and experiment was repeated twice. $^{**}P < 0.01$. $^{***}P < 0.001$. Significance was tested on unpaired 2-tailed Student *t* test. CMP = common myeloid progenitor; Ctrl = control; Ery A = basophilic erythroblasts; Ery B = basophilic and polychromatic erythroblasts; Ery C = orthochromatic erythroblasts; GMP = granulocyte-monocyte progenitors; HGB = hemoglobin; LK = Lin$^-$ c-Kit$^+$; HSCs = hematopoietic stem cells; LSK = Lin-negative Sca-1–positive c-Kit–positive; MEP = megakaryocyte-erythrocyte progenitor; MPP4 = multipotent progenitor population 4; PLT = platelets; RBC = red blood cells; WBC = white blood cells.

and progenitor cells (made of 796 single cells and quite homogeneous in terms of differential gene expression) underwent a limited proportional skewing, whereas lineage-primed precursors showed either a contraction (e.g., granulocytic and neutrophil precursors) or an expansion (e.g., common myeloid progenitor, B-cell precursors, and progenitors). These adaptations were limited primarily to the initial time points after ^{223}Ra treatment, whereas the reciprocal proportions were reestablished within 40 d from treatment (Fig. 4C), in line with flow cytometry data. To leverage the power of single-cell transcriptome data, we then examined differentially expressed genes from the clusters representing stem and early progenitors by comparing each posttreatment time point (days 4, 11, and 40) with the baseline (day 0). Gene ontology and pathway search via Gene Set Enrichment Analysis (*21–23*) on day 4 after treatment showed upregulation of genes related to apoptosis, radiation response, and double-strand break repair, reflecting an ionizing insult and need to react, which in hematopoietic stem and progenitor cell was overcome by day 40. An enrichment for terms related to metabolism, DNA replication, cell cycle, and hematopoietic stem/progenitor cell differentiation was also evident in most populations at early time points (Fig. 4D), indicating that the acute irradiation insult prompted progenitor cells to activate a mitogenic program to restore all hematopoietic types to their baseline levels. Interestingly, very few differences were identifiable at baseline and 40 d after treatment (Fig. 4D; Supplemental Fig. 8) in more immature populations, indicating that most perturbations at the transcriptomic level are fully resolved.

Overall, the data obtained at the single-cell level indicate that in all bone marrow populations. ^{223}Ra has an acute toxicity that is overcome by 40 d after treatment. This finding supports the notion that ^{223}Ra administration, although acutely toxic, does not permanently damage the hematopoietic system.

^{223}Ra Exposure Does Not Impair Full Hematopoietic Reconstitution

Given the transient myelotoxicity that affects all the hematopoietic compartments, we further investigated whether HSCs were able to fully reconstitute a functional steady-state hematopoiesis after acute exposure to ^{223}Ra. To this purpose, we performed bone marrow transplantation experiments using bone marrow from donors that were exposed to ^{223}Ra treatment. C57BL/6 GFP mice were treated with saline (as control) or ^{223}Ra; after 30 d their bone marrow was recovered and implanted in lethally irradiated wild-type C57BL/6 mice. Three-dimensional reconstruction of femurs at the multiphoton microscope 1 mo after treatment showed repopulation of the bone marrow cavity by GFP cells in both control and ^{223}Ra-exposed mice, whereas wild-type C57BL/6 mice did not show any specific fluorescence (Fig. 5A). Hematologic parameters (white blood cells, red blood cells, hemoglobin, platelets) were monitored as an index of functional bone marrow reconstitution 1 mo after transplantation, showing no differences between mice that were previously exposed to ^{223}Ra and those exposed to control treatment (Fig. 5B). Finally, both control and ^{223}Ra-exposed mice survived 40 wk after transplantation (Fig. 5C).

These results show that the acute ^{223}Ra insult to HSCs does not impair full hematopoietic reconstitution, thus indicating that the treatment does not subvert bone marrow function over the long term.

DISCUSSION

Among the limited treatments currently available for patients with castration-resistant prostate cancer metastatic to bone, ^{223}Ra is a viable option that improves overall survival coupled with a good therapeutic index and relatively low toxicity (*8*). Such results prompted further clinical testing of ^{223}Ra for the treatment of other primary cancers and cancers metastatic to bone, with an increasing number of patients who could benefit from this drug (*10–12*).

^{223}Ra exerts zonal cancer cell killing and efficiently reduces tumor mass in vivo, especially in the case of small lesions (*4,7*), and its preventive application decreases tumor burden in preclinical models of disseminated breast cancer (*10*). In addition, retrospective clinical analyses showed that overall survival is improved in men with metastatic bone disease and a low bone scan index

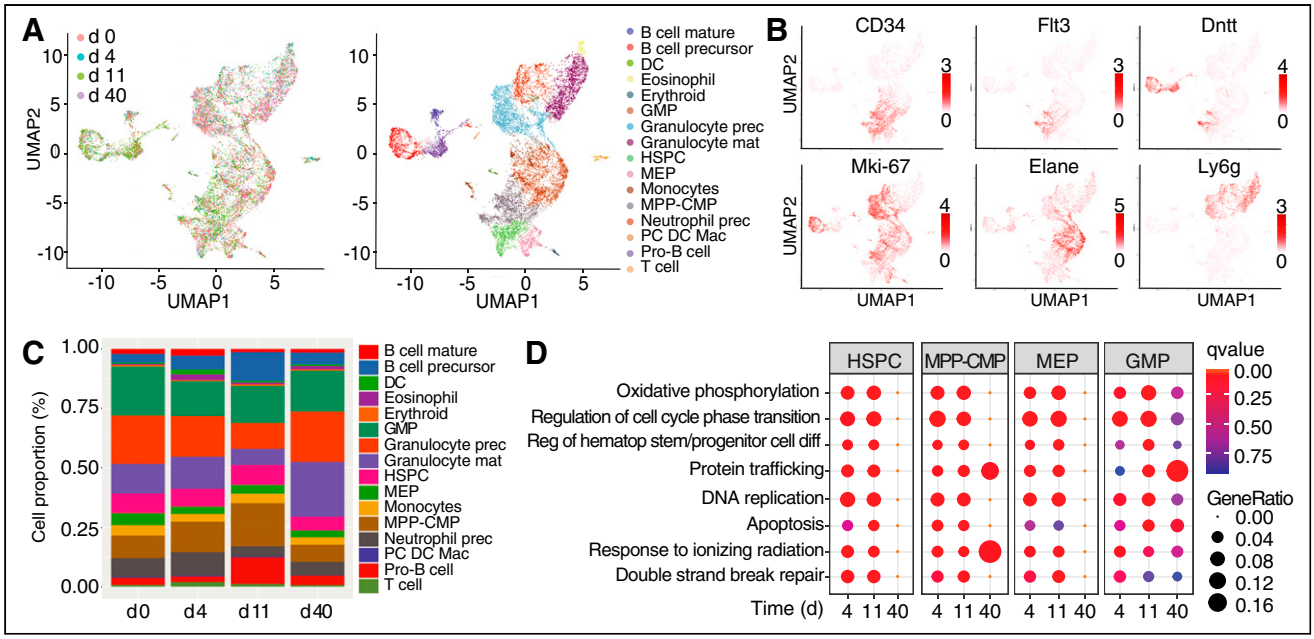

FIGURE 4. ^{223}Ra treatment induces temporary changes in bone marrow cell transcriptome. (A) Uniform manifold approximation and projection of single-cell RNA-sequencing data collected from Kit-positive bone marrow cells of C57/BL6 mice before treatment (day 0) and after 4, 11, and 40 d of treatment with ^{223}Ra in 3 mice per group. (B) Uniform manifold approximation and projection of color-coded hematopoietic populations, based on single-cell transcriptomic profiles. (C) Expression pattern of selected key marker genes. Color scale indicates log-normalized expression levels of indicated genes. (D) Relative proportion of 16 individual cell populations over time after treatment with ^{223}Ra for 0 (untreated), 4, 11, and 40 d. (E) Dot plots showing most representative gene sets from top differentially expressed genes in mice treated with ^{223}Ra for 4, 11, and 40 d vs. untreated. Size of dots represents proportion of differential expressed genes in each term, and color indicates significance of enrichment. DC = dendritic cells; diff = differentiation; GMP = granulocyte-monocyte progenitors; hematop = hematopoietic; HSPC = hematopoietic stem and progenitor cell; MEP = megakaryocyte/erythroid progenitors; MPP-CMP = multipotent progenitors-common myeloid progenitors; PC DC Mac = plasma cell dendritic cell macrophage mixed markers; reg = regulation; UMAP = uniform manifold approximation and projection.

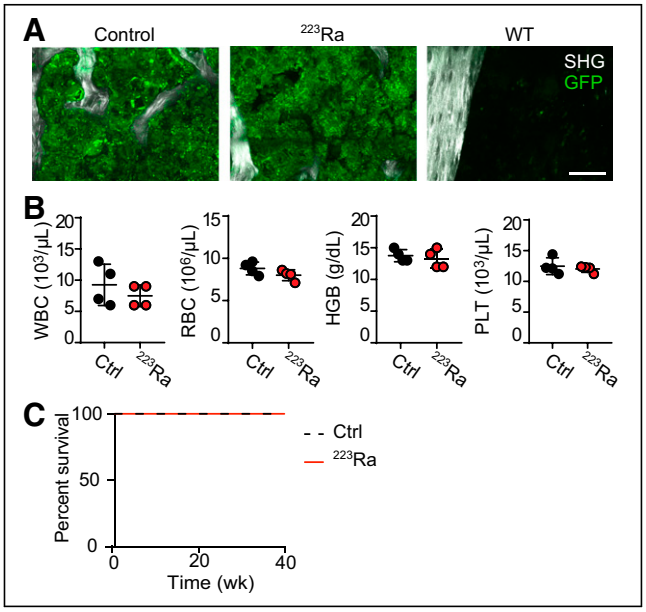

FIGURE 5. ^{223}Ra does not affect long-term functionality of HSCs. (A) Bone marrow reconstitution in mice administered control or ^{223}Ra-exposed bone marrow cells monitored by immunofluorescence analysis 1 mo after transplantation. Wild-type GFP mouse tibia is shown as negative control. Scale bar is 100 μm. (B) Hematologic analysis of transplanted mice. Mean ± SD is shown for 4 mice per group. (C) Survival of control or ^{223}Ra-exposed transplanted mice (n = 4). Ctrl = control; HGB = hemoglobin; PLT = platelets; RBC = red blood cells; SHG = second-harmonic generation; WBC = white blood cells; WT = wild type.

(*24*), whereas preliminary clinical observations suggest that ^{223}Ra has higher efficiency in individuals with fewer circulating tumor cells (<5 circulating tumor cells/7.5 mL of blood) (*25*). Altogether, this evidence supports ^{223}Ra application for secondary prevention of bone metastasis and treatment of oligometastatic bone disease to achieve maximal efficacy, extending the benefits of this treatment to patients at early stages.

Recent clinical observations showed that ^{223}Ra does not induce the emergence of secondary malignancies (*13,14*), and neutropenia and thrombocytopenia are among the most common side effects (*15*). To exclude long-term myelotoxicity, which is particularly relevant when considering a larger cohort of patients with longer survival expectancy, we tested the global effects of ^{223}Ra exposure on hematopoiesis in preclinical models. We confirmed that ^{223}Ra incorporation within bone-calcified matrix induces cellular changes in the bone marrow. Topologic alterations were induced in the bone marrow cavity, where zonal radiologic damage emerged 4 d after treatment and decreased over time up to day 40 after treatment, paralleled by an increment of adipocytes. Cytotoxicity, which extended among all hematopoietic cell lineages, was overcome by 6 wk from ^{223}Ra administration and was paralleled by a significant, transient decrease in circulating white blood cells, with a 50% reduction 28 d after treatment compared with control-treated mice. In patients 4 wk after the first dose of ^{223}Ra, the levels of circulating neutrophils significantly decreased by approximately 25% (*15*). The higher cytotoxic impact in mouse models might be explained by the smaller scale of mouse bones compared with human ones, which in proportion are exposed to higher levels of α-radiation (that travels for <100 μm of distance (*8*)).

Blood cells are formed in a complex microenvironment in which several different stromal cell types (such as endothelial, osteoblastic, and adipogenic progenitors) foster hematopoiesis through mutual interactions. This delicate balance is compromised by external insults, such as chemotherapy or radiation (*18*), which impact the hematopoietic compartment both directly (by arresting its proliferation) and indirectly (by compromising its niche (*26–28*)). ^{223}Ra induces zonal bone marrow injury at the tibia epiphysis and metaphysis, paralleled by the transient change in the number of peripheral blood cells. This early damage is followed by a marked increase in adipocytes, which usually accompanies the restoration of normal hematopoiesis. This increase is in line with recent studies showing that irradiation or fluorouracil treatment causes differentiation of stromal cells into adipocytes, which in turn produce cytokines that stimulate HSCs to regenerate hematopoiesis (*20*). Bone marrow alterations were evident at the epiphysis or metaphysis, where dense trabecular areas are present, and more prominent remodeling of cancellous bone (*29*) may further increase ^{223}Ra incorporation, enhancing zonal toxicity. In contrast, the diaphysis was relatively unaltered. Consistently, high-resolution analysis of bone by α-camera autoradiography showed a predominant ^{223}Ra localization at the growth plate, with little activity at the diaphysis and no signal from the bone marrow (*2*). Interestingly, most quiescent long-term HSCs preferentially reside in the diaphysis, and in particular within perivascular rather than osteoblastic niches (*30*), suggesting a potential role for the region-specific distribution of ^{223}Ra in sparing some niches that host HSCs.

Importantly, our results show no major differences in lineage commitment at baseline and 40 d after ^{223}Ra treatment—neither in the transcriptional programs of the hematopoietic stem and progenitor cells nor in their mature progeny. The bone marrow of mice exposed to ^{223}Ra efficiently restores full hematopoiesis in irradiated hosts, with no significant differences from control-treated mice. This finding suggests that, despite transient bone marrow damage, HSC functionality and normal hematopoietic reconstitution processes are not permanently impaired by ^{223}Ra. Our study addressed these effects after exposure to 1 therapeutic dose of ^{223}Ra, and follow-up work can be performed to exclude a potential increased cytotoxicity by repeated cycles of treatment or by exposure to higher doses.

CONCLUSION

Our results provide a comprehensive explanation of the effects of ^{223}Ra on bone marrow cells and suggest their reversibility, excluding long-term myelotoxicity.

DISCLOSURE

This work was supported by the University of Texas M.D. Anderson Cancer Center Prostate Cancer SPORE (P50 CA140388-09) and Moonshots Initiative; Bayer HealthCare Pharmaceuticals (57440); the U.S. National Institutes of Health (R01CA202025, R01CA202027, R01CA216421, R01CA228135; P01CA229086, and P30 CA016672); the Leukemia & Lymphoma Society (TRP 6580); Alex's Lemonade Stand Foundation for Childhood Cancer; and St. Baldrick's Cancer Research Foundation. ^{223}Ra was received from Bayer. No other potential conflict of interest relevant to this article was reported.

ACKNOWLEDGMENTS

We thank Drs. Maria Guillamot-Ruano and Lara Brambilla (NYU Langone Health) for critical reading of the manuscript and the Leukemia Sample Bank at University of Texas M.D. Anderson Cancer Center for sharing the ABX Micros 60 instrument.

KEY POINTS

QUESTION: Does ^{223}Ra induce permanent bone marrow damage?

PERTINENT FINDINGS: ^{223}Ra prolongs survival in bone-metastasis patients but induces significant neutropenia. Three-dimensional multiphoton microscopy, fluorescence-activated cell sorting analysis, single-cell RNA sequencing, and bone marrow transplantation reveal reversible ^{223}Ra-mediated functional myelotoxicity.

IMPLICATIONS FOR PATIENT CARE: Our results provide a comprehensive explanation of ^{223}Ra reversible effects on bone marrow cells and exclude long-term myelotoxicity, supporting safety for patients.

REFERENCES

1. Bruland ØS, Nilsson S, Fisher DR, Larsen RH. High-linear energy transfer irradiation targeted to skeletal metastases by the alpha-emitter ^{223}Ra: adjuvant or alternative to conventional modalities? *Clin Cancer Res.* 2006;12:6250s–6257s.
2. Abou DS, Ulmert D, Doucet M, Hobbs RF, Riddle RC, Thorek DL. Whole-body and microenvironmental localization of radium-223 in naive and mouse models of prostate cancer metastasis. *J Natl Cancer Inst.* 2015;108:djv380.
3. Gandaglia G, Abdollah F, Schiffmann J, et al. Distribution of metastatic sites in patients with prostate cancer: a population-based analysis. *Prostate.* 2014;74:210–216.
4. Dondossola E, Casarin S, Paindelli C, et al. Radium 223-mediated zonal cytotoxicity of prostate cancer in bone. *J Natl Cancer Inst.* 2019;111:1042–1050.
5. Paindelli C, Navone N, Logothetis CJ, Friedl P, Dondossola E. Engineered bone for probing organotypic growth and therapy response of prostate cancer tumoroids in vitro. *Biomaterials.* 2019;197:296–304.
6. Suominen MI, Fagerlund KM, Rissanen JP, et al. Radium-223 inhibits osseous prostate cancer growth by dual targeting of cancer cells and bone microenvironment in mouse models. *Clin Cancer Res.* 2017;23:4335–4346.
7. Paindelli C, Casarin S, Wang F, et al. Enhancing radium 223 treatment efficacy by anti-beta 1 integrin targeting. *J Nucl Med.* October 28, 2021 [Epub ahead of print].
8. Parker C, Nilsson S, Heinrich D, et al. Alpha emitter radium-223 and survival in metastatic prostate cancer. *N Engl J Med.* 2013;369:213–223.
9. Sartor O, Coleman R, Nilsson S, et al. Effect of radium-223 dichloride on symptomatic skeletal events in patients with castration-resistant prostate cancer and bone metastases: results from a phase 3, double-blind, randomised trial. *Lancet Oncol.* 2014;15:738–746.
10. Suominen MI, Rissanen JP, Kakonen R, et al. Survival benefit with radium-223 dichloride in a mouse model of breast cancer bone metastasis. *J Natl Cancer Inst.* 2013;105:908–916.
11. Ueno NT, Tahara RK, Fujii T, et al. Phase II study of radium-223 dichloride combined with hormonal therapy for hormone receptor-positive, bone-dominant metastatic breast cancer. *Cancer Med.* 2020;9:1025–1032.
12. Morris MJ, Corey E, Guise TA, et al. Radium-223 mechanism of action: implications for use in treatment combinations. *Nat Rev Urol.* 2019;16:745–756.
13. Parker CC, Coleman RE, Sartor O, et al. Three-year safety of radium-223 dichloride in patients with castration-resistant prostate cancer and symptomatic bone metastases from phase 3 randomized Alpharadin in Symptomatic Prostate Cancer trial. *Eur Urol.* 2018;73:427–435.
14. Dizdarevic S, Petersen PM, Essler M, et al. Interim analysis of the reassure (radium-223 alpha emitter agent in non-intervention safety study in mCRPC population for long-term evaluation) study: patient characteristics and safety according to prior use of chemotherapy in routine clinical practice. *Eur J Nucl Med Mol Imaging.* 2019;46:1102–1110.
15. Vogelzang NJ, Coleman RE, Michalski JM, et al. Hematologic safety of radium-223 dichloride: baseline prognostic factors associated with myelosuppression in the ALSYMPCA trial. *Clin Genitourin Cancer.* 2017;15:42–52.e8.
16. Hermiston ML, Zikherman J, Zhu JW. CD45, CD148, and Lyp/Pep: critical phosphatases regulating SRC family kinase signaling networks in immune cells. *Immunol Rev.* 2009;228:288–311.
17. Tsai C-K, Wang T-D, Lin J-W, et al. Virtual optical biopsy of human adipocytes with third harmonic generation microscopy. *Biomed Opt Express.* 2013;4:178–186.

18. Butler A, Hoffman P, Smibert P, Papalexi E, Satija R. Integrating single-cell transcriptomic data across different conditions, technologies, and species. *Nat Biotechnol.* 2018;36:411–420.
19. Giladi A, Paul F, Herzog Y, et al. Single-cell characterization of haematopoietic progenitors and their trajectories in homeostasis and perturbed haematopoiesis. *Nat Cell Biol.* 2018;20:836–846.
20. Naveiras O, Nardi V, Wenzel PL, Hauschka PV, Fahey F, Daley GQ. Bone-marrow adipocytes as negative regulators of the haematopoietic microenvironment. *Nature.* 2009;460:259–263.
21. Hänzelmann S, Castelo R, Guinney J. GSVA: Gene set variation analysis for microarray and RNA-seq data. *BMC Bioinformatics.* 2013;14:7.
22. Liberzon A, Birger C, Thorvaldsdóttir H, Ghandi M, Mesirov JP, Tamayo P. The molecular signatures database (MSigDB) hallmark gene set collection. *Cell Syst.* 2015;1:417–425.
23. Barbie DA, Tamayo P, Boehm JS, et al. Systematic RNA interference reveals that oncogenic KRAS-driven cancers require TBK1. *Nature.* 2009;462:108–112.
24. Alva A, Nordquist L, Daignault S, et al. Clinical correlates of benefit from radium-223 therapy in metastatic castration resistant prostate cancer. *Prostate.* 2017;77:479–488.
25. Carles J, Castellano D, Méndez-Vidal MJ, et al. Circulating tumor cells as a biomarker of survival and response to radium-223 therapy: experience in a cohort of patients with metastatic castration-resistant prostate cancer. *Clin Genitourin Cancer.* 2018;16:e1133–e1139.
26. McCulloch EA, Till JE. The radiation sensitivity of normal mouse bone marrow cells, determined by quantitative marrow transplantation into irradiated mice. *Radiat Res.* 1960;13:115–125.
27. Xie Y, Yin T, Wiegraebe W, et al. Detection of functional haematopoietic stem cell niche using real-time imaging. *Nature.* 2009;457:97–101.
28. Otsuka K, Hirabayashi Y, Tsuboi I, Inoue T. Regeneration capability of Lin-/*Kit*+/Sca-1+ cells with or without radiation exposure for repopulation of peripheral blood in lethally irradiated mice monitored using Ly5.1 isotype on days 35, 90, and 270 after transplantation. *Exp Hematol.* 2010;38:417–425.
29. Langdahl B, Ferrari S, Dempster DW. Bone modeling and remodeling: potential as therapeutic targets for the treatment of osteoporosis. *Ther Adv Musculoskelet Dis.* 2016;8:225–235.
30. Acar M, Kocherlakota KS, Murphy MM, et al. Deep imaging of bone marrow shows non-dividing stem cells are mainly perisinusoidal. *Nature.* 2015;526:126–130.